Computers in Biology and Medicine 104 (2019) 227–234

Contents lists available at ScienceDirect

Computers in Biology and Medicine

journal homepage: www.elsevier.com/locate/compbiomed

A two-dimensional (2D) systems biology-based discrete liver tissue model: A simulation study with implications for ultrasound elastography of liver fibrosis

Yu Wang[a], Jingfeng Jiang[a,b,*]

[a] Department of Biomedical Engineering, Michigan Technological University, Houghton, MI, 49931, USA
[b] Department of Mechanical Engineering and Engineering Mechanics, Michigan Technological University, Houghton, MI, 49931, USA

ARTICLE INFO

Keywords:
Liver fibrosis
Steatosis
Agent-based modeling
Ultrasound elastography
Ultrasound tissue characterization

ABSTRACT

Continuum tissue models that were often used to simulate or analyze the mechanical properties of tissues being imaged may not be biologically realistic. Our primary objective was to establish the feasibility of using systems biology to construct biologically relevant tissue models linking tissue structure, composition and architecture to the ultrasound measurements directly. The first application was designated to model fibrotic liver tissues.

The proposed liver tissue model leveraged established histopathology knowledge of fibrotic liver tissues. Particularly, rules of systems biology derived from molecular histopathology were first implemented into an agent-based software platform SPARK to reflect progressions of liver fibrosis with/without steatosis. Then, microscopic compositions of tissues (*e.g.* cellular components) were converted to computing grids (at the 50–100 μm scale) for wave simulations using an open-source K-Wave. To verify the physical soundness of the proposed model, virtual wave speed measurements (*i.e.* shear wave speed [SWS] and the speed of sound [SOS]) were performed.

Our initial results demonstrated that the simulated SWS values increased with the progression of liver fibrosis (from 1.5 m/s [Fibrosis stage 1] to 4 m/s [Fibrosis stage 4]). Similarly, the simulated SOS values were within the range of clinical data (from 1575 m/s [Fibrosis stage 0–3] to 1594 m/s [Fibrosis stage 4]).

In summary, we found that those systems biology simulated fibrotic liver tissues with and without steatosis can reflect spatial characteristics of relevant histology. Also, their mechanical characteristics (*i.e.* shear/compressional wave speed) were in good agreement with data reported in the clinical literature.

1. Introduction

Ultrasound elastography [1] aims at non-invasively measuring tissue stiffness by tracking the motion of soft tissues and has demonstrated its values in multiple organ systems for clinical diagnosis and therapeutic interventions [2]. Generally, in elastography, appropriate constitutive models are explicitly or implicitly required to convert or interpret elastographic measurements (*e.g.* displacements, strain, shear wave speed) to mechanical properties (*e.g.* Young's/Shear modulus). Although the linearly elastic model is still in the mainstream, micro-mechanics-based [3], hyperelastic [4–6], viscoelastic [7,8] and anisotropic [9,10] models have also been adopted to inversely analyze tissue elasticity.

Furthermore, researchers are also actively seeking to establish the mechanistic link between the microstructure of biological tissues and their macroscopic material properties using elastography measurements. Models of this kind could potentially open new avenues for correlating radiological findings with pathological changes. Notably, the work by Sack et al. examined how constants of the viscoelastic power-law measured by elastography can be related to the mechanical properties of cellular networks [11]. This was accomplished by assuming a fractional derivative-based viscoelastic model in which the fractional order could be linked to the cellular network. Prof. Parker introduced a microchannel flow model in which the fluid outflow from micro-vessels under the applied stress can be used to explain frequency-dependent shear wave dispersion in soft, isotropic, vascularized tissues [12,13]. However, these two studies mentioned above were still based on continuum mechanics models.

In the pioneering work from Prof. Waag's group [14], a two-dimensional anatomically accurate model was first derived from

* Corresponding author. Material and Mineral Engineering Building 309, Department of Biomedical Engineering, Michigan Technological University Houghton, MI, 49931, USA.
E-mail address: jjiang1@mtu.edu (J. Jiang).

https://doi.org/10.1016/j.compbiomed.2018.11.027
Received 7 September 2018; Received in revised form 30 November 2018; Accepted 30 November 2018
0010-4825/

histology data and then used to understand how the ultrasound wave was distorted after passing the chest wall. Of note, this discrete tissue model containing sub-wavelength tissue heterogeneities was able to more realistically simulate the interaction between the tissue and acoustic wave, as compared to other numerical acoustic simulations done using continuum models. As inspired by this early success [14], a discrete (microstructural) liver tissue model is proposed here to investigate shear wave propagation in fibrotic liver tissues; main constituents of the proposed model are collagen fibers, fatty deposits, and a ground matrix. Unlike the previous study by Mast et al. [14], the proposed discrete model was derived from systems biology.

In this study, the utility of this novel approach was demonstrated through "simulated" elastographic measurements in fibrotic liver tissues. We first derived a systems-biology-based (SB) liver tissue model, pathologically replicating the progress of liver fibrosis. More specifically, we generated two-dimensional (2D) virtual fibrotic liver tissues mimicking the liver fibrosis due to insults induced by Carbon tetrachloride (CCL_4). Those systems-biology-based virtual tissues could histopathologically resemble different stages of liver fibrosis with and without steatosis [15,16]. Then, we evaluated how the proposed fibrotic liver tissue model could predict experimental wave measurements (*i.e.* sound of speed [SOS] and shear wave speed [SWS]). In other words, *in vivo* results available were compared to computer simulation results in this feasibility study as preliminary validations.

Toward this end, the rest of this paper is organized as follows. We began the Methods and Materials Section with the description of the virtual liver tissue model, followed by detailed descriptions of performing subsequent computer simulations using K-WAVE [17]. The proposed virtual fibrotic liver tissue model with and without liver steatosis was integrated into all numerical models. In the Results Section, virtual wave speed measurements were performed to validate the proposed model using *in vivo* data available in the literature. We concluded this study by a brief discussion.

2. Materials and methods

As shown in Fig. 1, interactions between the SB based virtual liver tissue model and simulations of compression and shear wave propagation involve several major steps. All steps, along with the use of two open-source simulation platforms, namely a wave simulator (K-WAVE [17]) and an agent-based knowledge simulator (SPARK [18]), are briefly presented below.

2.1. Virtual liver tissue model

We treated the fibrotic liver tissue as a three-phase random medium where the normal liver parenchyma and the deposits of excessive connective collagen tissues and lipids are the background and inclusions, respectively. Architectural features of those three components were simulated using SB. In order to do so, we expanded and modified an existing agent-based SB model of liver fibrosis originally developed by others [19] in SPARK. Signaling pathways for liver fibrosis, liver steatosis, and interactions between the liver fibrosis and steatosis are shown in Fig. 2. We first describe simulations of liver fibrosis and steatosis as two independent processes and then outline their interactions on knowledge available [20]. More details can be found in Appendix A (Supplemental Material).

Toxicity based liver fibrosis, due to the injection of carbon tetrachloride (CCL_4), was induced through four parallel schemes (Fig. 2). In the first scheme, liver injuries induced by CCL_4 transform normal hepatocytes into dead agents. In the second scheme, once Kupffer cells sense dead hepatocytes, they immediately phagocytize and activate the production of TNF-α (a canonical pro-inflammatory cytokine) and TGF-β1 (a canonical anti-inflammatory cytokine). In the third scheme, assuming inadequate clearance of dead hepatocytes occurs, damage-associated molecular pattern (DAMP) molecules such as HMGB1 starts to accumulate. Certainly, the presence of HMGB1 would subsequently recruit and convert more monocytes to active Kupffer cells. In the fourth scheme, agents such as active portal fibroblasts and HSCs transform to myofibroblast agents when they detect TNF-α. Similarly, when the system detects TGF-β1, myofibroblast agents start to proliferate and deposit collagen into existing ECM structure. Of note, in all four above-mentioned schemes, interactions among them were probabilistic.

Now referring to the simulation of liver steatosis, we adopted a theoretical model developed by Schleicher et al. [21]. More specifically, the active scheme (hereafter referred as to the fifth scheme) [21] is that the storage of triacylglycerol (TAG) within hepatocytes leads to cell enlargement, thereby reducing the sinusoids radius and impairing hepatic microcirculation. Because of the compromised microcirculation, oxygen supplies will be reduced and, consequently, lipid oxidation will be further impaired. Eventually, lipid accumulation will occur in the liver (Fig. 2). Currently, the dynamic interactions between the liver steatosis and fibrosis are complex and not fully understood. Based on work by Diehl et al. [22], we assumed that the presence of lipid droplets up-regulates TNF-α . As a multi-functional cytokine, TNF- α is actively involving in energy metabolism, especially lipid homeostasis. This interaction is also illustrated in Fig. 2.

2.2. Use of the virtual tissue model for simulations of ultrasound compressional/shear waves

2.2.1. Creation of computing grid

After the above-mentioned SB simulations, these resultant tissues were represented by aggregates of non-overlapping, circular particles. In other words, an SB-based simulation resulted in a random multiple-phase medium (Fig. 1b), in which hepatocytes (radius: 50 μm), lipid cells (radius: 40 μm) and collagen depositions (50 μm X 30 μm) all occupied the physical space. Then, an image-based "conversion" scheme (Fig. 3a to Fig. 3b) was used to convert the random multiple-phase medium into a discrete liver tissue model as follows. Basically, all SB simulation results were saved as a JPEG image whose pixel size is

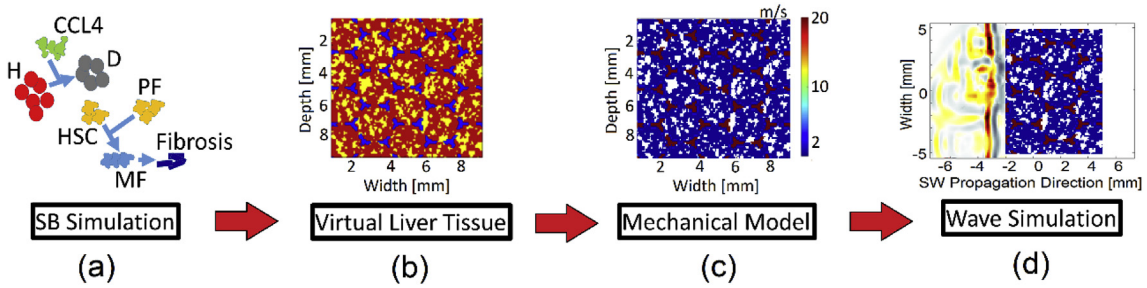

Fig. 1. Schematic illustrations of the workflow: (a) Systems biology [SB] simulation, (b) virtual liver tissue generated from SB simulation, (c) mechanical model of the virtual liver tissue and (d) wave simulations by K-WAVE. The wave propagates from left to right in (d). In (a), different color represents different agents whose acronyms can be in Fig. 2, while red, blue and yellow represent normal liver tissue, fibrosis, and fat, respectively in (b). In (c), the color bar denotes SWS in m/s.

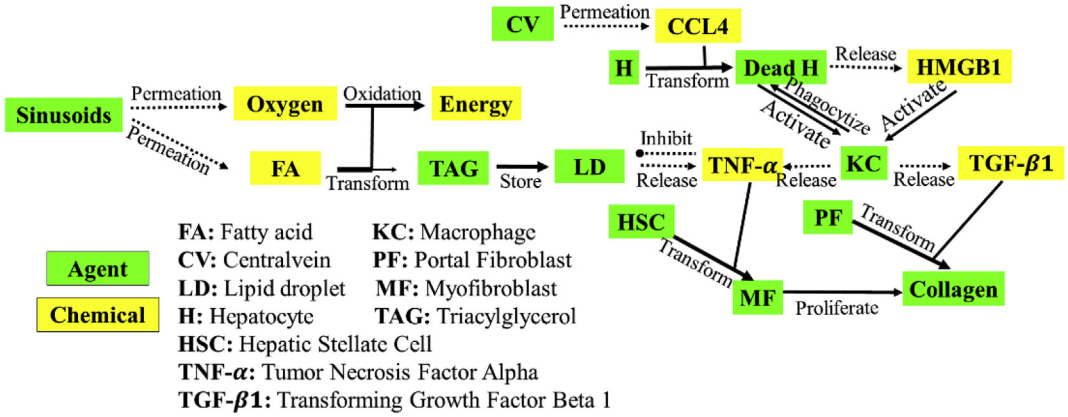

Fig. 2. A diagram showing signaling pathways related to liver fibrosis and steatosis induced by CCL_4 insults induced liver fibrosis and lipid accumulation, respectively.

0.014 mm. The JPEG image was then decimated to a computing grid whose grid space was either 0.1 mm (7 × 7 to 1; ultrasound compressive wave simulations) or 0.1 mm (7 × 7 to 1; plane shear wave simulations). The 50-μm grid spacing was approximately 1/9 of the ultrasound wavelength at 2 MHz, while the 100-μm grid spacing is roughly 1/100 of the wavelength of the shear wave.

Mechanical properties (*e.g.* speed of sound and shear wave speed) were assigned to each point on the discrete computing grid (Fig. 3c). The computing grid could be directly used by K-Wave [17] to solve wave equations using a K-space finite difference scheme.

2.2.2. Virtual wave simulations

A uniform 90 mm (along the wave propagation direction) × 22 mm computing domain was used to generate wave speed data, as shown in Fig. 4. A 20 mm × 20 mm central rectilinear region of interest (ROI) containing the proposed virtual liver tissues (Fig. 3c) was embedded into the computing domain. The wave propagation was simulated by K-Wave [17].

For each model, one transient cycle of plane shear or compressional wave excitation at 100 Hz or 2 MHz, was applied to a set of locations close to the left edge of the ROI (see the green line in Fig. 4) to initiate the shear/compressional wave propagation. Both frequencies are consistent with those used in a clinical setting [1,23]. Periodic boundary conditions have been appropriately configured to avoid reflection on the boundaries. Details of the simulation setting can be found in our previous papers [27]. Simulation parameters (Table 1) were adopted from the literature [24–27].

As shown in Table 1, the normal liver shear modulus was set to be around 1.96 kPa (equivalent to the SWS of 1.4 m/s) [26]. The shear modulus of the fatty tissues in Table 1 was similar to those of abdominal fat [24]. The shear modulus value of fibrotic liver tissues was elevated to be around 400 kPa (equivalent to SWS of 20 m/s) [25]. Because, to our knowledge, there is no mechanical testing data available for fibrotic (collagenous) liver tissues at the spatial scale of 50–100 μm, the micropacket of fibrotic tissues was chosen to be close to the shear modulus values of arterial tissues.

2.2.3. Compositions of virtual fibrotic livers

The METAVIR scores clinically [28] classify the liver tissue into five stages: F0 − F4. F0 denotes normal liver tissues, and F1−F4 represent levels of liver fibrosis. Stages F1 and F2 were considered as the early stages of liver fibrosis, and stages F3 and F4 were regarded as the late stages of liver fibrosis.

The collagen proportionate area (CPA) ratios are typically reported in conjunction with METAVIR classifications. Because detailed statistical analyses of CPA ratios were not available, we assumed that the CPA ratio follows a Gaussian distribution and subsequently derived its mean and standard deviation based on available data [29,30] for each fibrosis stage, as shown in Table 2.

The area fraction of each component and two-point correlation length (CL) were calculated from all microscopic tissue distributions (Fig. 3c). The CL of r represents a distance from which the probability of finding two points in the same (material) phase separated by a distance r drops to a stable but low plateau (*e.g.* 0.2). In the other words, the two-point CL [31] is used to spatially characterize this multiphase tissue model.

As shown in Table 3, in order to simulate one (METAVIR) fibrosis stage, three different CPA ratios were first used. Then, simulation results were reweighted when the final simulation results were calculated. The weighting (Table 3) was to ensure that the weighted CPA distribution under the fibrosis stage followed the assumed Gaussian distribution as shown in Table 2. Hence, 9 different realizations were

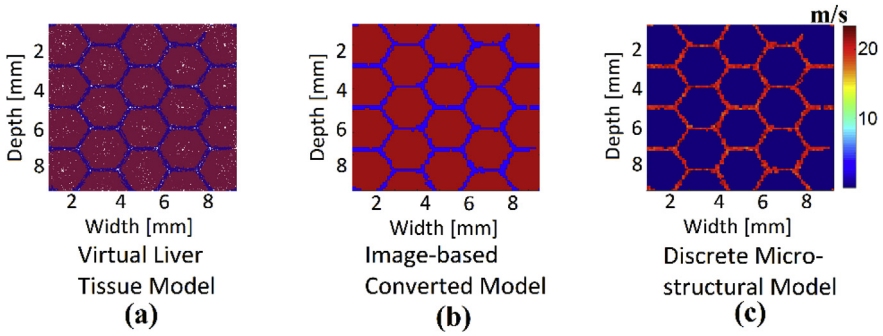

Fig. 3. An illustration of the process of model conversion: (a) the original model generated by SPARK, (b) a converted model by "decimation" from (a) and (c) a discrete micro-structural model. In (c), the color bar represents SWS in m/s.

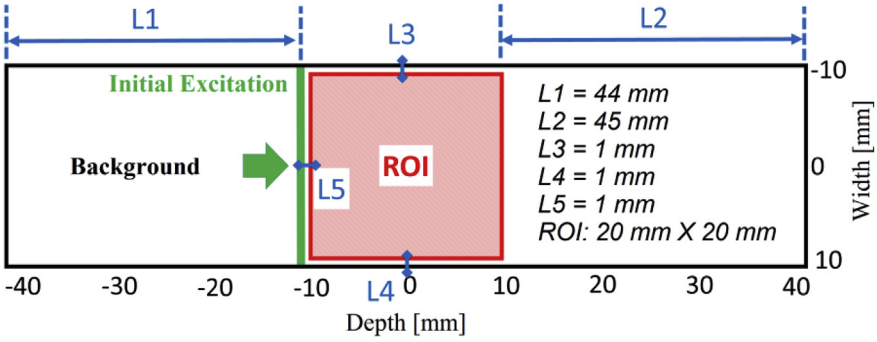

Fig. 4. An illustration of computing domain used for all K-Wave simulations. A (20 mm × 20 mm) region of interest (ROI) containing simulated virtual liver tissues was embedded into a larger (90 mm × 22 mm) uniform background. The green vertical line indicates the location of initial mechanical vibration, while the green arrow represents the wave propagation direction. For shear and compression wave propagations, the initial excitations are vertical and parallel to the wave propagation direction, respectively.

Table 1
A list of properties of the virtual liver tissues used in the K-WAVE simulations.

	Normal Liver Tissue	Collagen Deposition	Fat
SWS (m/s)	1.4 ± 0.1	20 ± 1.5	0.8 ± 0.04
SOS (m/s)	1540 ± 10	1800 ± 10	1450 ± 10
Mass Density (kg/m^3)	1000 ± 20	1300 ± 30	1000 ± 20

Table 2
Derived CPA values for 4 METAVIR stages (F1 to F4).

METAVIR stage	F1		F2		F3		F4	
	Mean	STD	Mean	STD	Mean	STD	Mean	STD
CPA (%)	5	3	8	5	11	6	21	6

Table 3
A list of simulation configurations used in K-WAVE simulations. The weights listed were calculated so that the weighted CPA distribution of each fibrosis stage followed its respective Gaussian distribution (Table 2).

METAVIR stage	CPA (%)	CL (mm)	Realizations	Total Data Points	Weight
F1	2	0.6	3	6480	23%
	4	0.9	3	6480	46%
	7	0.9	3	6480	31%
F2	5	0.6	3	6480	33%
	8	1.2	3	6480	38%
	12	1.3	3	6480	29%
F3	6	0.6	3	6480	31%
	11	1.3	3	6480	44%
	17	1.4	3	6480	25%
F4	15	1.3	3	6480	27%
	20	1.4	3	6480	47%
	27	1.5	3	6480	26%

used for each simulated liver fibrosis stage. Especially, each realization can generate 2160 data points of wave speed (*i.e.* SWS and SOS). Each CPA can generate 6480 (2160 × 3) data points. Then, we randomly select data points from each CPA based on weights shown in Table 3 to generate the final data points. To show how the presence of liver steatosis can affect the ultrasound measurements, moderate simulated liver steatosis (*i.e.* a fat area fraction of 50% [20]) was simultaneously simulated along with liver fibrosis following the signaling pathways described in Fig. 2, if necessary.

2.3. Validations using available clinical data

Table 4 summarizes the liver stiffness values of four METAVIR stages obtained from 6 peer-reviewed publications in which TE was used; the number of patients associated with each METAVIR stage is also provided in Table 4. Because of the raw SWS data were not available, computer-synthesized SWS data derived from those six studies were generated as follows. Random SWS velocity data for each

Table 4
Liver stiffness (Young's Modulus; Mean ± one standard deviation) summarized from 6 published transient elastography (TE) studies (hereafter referred to Studies 1 to 6).

	Estimated Liver Stiffness (kPa) (METAVIR stage)			
	F1 (kPa) (Patient No.)	F2 (kPa) (Patient No.)	F3 (kPa) (Patient No.)	F4 (kPa) (Patient No.)
Study 1 [49]	6.02±1.58 (23)	8.3±2.02 (17)	12.52±3.0 (9)	22.41±7.55 (12)
Study 2 [50]	6.6±1.5 (82)	7.9±1.7 (82)	12.4±3.10 (23)	24.2±6.78 (28)
Study 3 [51]	6.6±2.6 (24)	7.4±3 (21)	11±7.6 (14)	17.2±12.1 (11)
Study 4 [52]	5.6±1.8 (46)	6.6±1.8 (18)	14.9±10.3 (9)	25.6±12.9 (46)
Study 5 [53]	4.5±1.3 (102)	6.6±1.1 (61)	8.9±0.9 (26)	15.1±7.8 (14)
Study 6 [54]	5.8±1.8 (19)	11.3±6.8 (39)	11.8±6 (30)	23.4±16.5 (19)

study were first generated by assuming that the SWS measurements in each study followed a Gaussian distribution. Then, synthesized SWS data from three studies were assembled such that the contribution of each clinical study was proportional to the number of patients available for the study. For instance, there were 5920 "computer-synthesized" SWS measurements for F1; among them, 460, 1640, 480, 920, 2040 and 380 were from Studies 1 to 6, respectively. The clinical SOS data (Table 5) were obtained from a study by Boozari et al. [23] Boozari et al. used a commercial scanner (Zonare Medical Systems, Inc, Mountain View, CA, USA) equipped with a curvilinear array transducer (C5–2).

2.4. Parameters involving in systems biology simulations

The above-mentioned SB (SPARK) simulation consists of multiple sequential steps. In each step, all chemical and biological agents (see Fig. 2) are updated. Major parameters used in the above-mentioned SB (SPARK) simulations are listed in Table 6 and those parameters can be largely divided into two categories: (1) parameters related to the life cycle and (2) parameters defining mobility. More specifically, the life cycle was defined as the lifespan of chemical and biological agents and its unit was the simulation step. The mobility of biological and chemical agents was slightly different. The mobility of a biological agent denoted a distance traveled by the agent between two adjacent simulation steps and its unit was mm/step. The mobility of a chemical agent was a surrogate of the diffusion rate. The rectilinear simulation domain was conventionally divided into squares. When a square was completely filled (100%) with a chemical agent A at the *i*th simulation step, the

Table 5
SOS measurements reported in fibrotic livers [23].

METAVIR stage	F0–F3	F4
SOS (m/s)	1575±21	1594±18

Table 6
A list of selected parameters used in the SB simulations.

Parameter (unit)	Value In Simulation
CCL_4 Diffusion Rate (/step)	50%
HMGB1 Diffusion Rate (/step)	50%
TNF-α Diffusion Rate (/step)	50%
TGF-β1 Diffusion Rate (/step)	50%
Fat Diffusion Rate (/step)	50%
Fat Inhibit Probability	50%
Stellate Move Speed (mm/step)	0.1
Hepatocyte Move Speed (mm/step)	0.1
Macrophage Move Speed (mm/step)	0.1
Hepatocyte Life Cycle (step)	90

mobility (or the diffusion rate) of A was the percentage occupancy of the agent A in the square's eight (8) immediate neighbors at the $(i+1)^{th}$ simulation step.

Using the parameters listed in Table 6 as the input, the collagen and lipid depositions were the output. The SPARK simulations stopped if an area percentage of collagen and/or lipid depositions (Table 7) would be reached. The sensitivity of the parameters listed in Table 6 can be found in Appendix B (Supplemental Material).

2.5. Data analysis

A lateral time-to-peak (TTP) algorithm [32] was adopted to estimate wave speeds (*i.e.* both SWS and SOS) along the respective wave propagation directions. The processing kernel length was 0.4 mm. To verify the kernel length sensitivity for the simulated wave speed, our results were reprocessed using a processing kernel length of 1.2 mm. We found that the means of wave speed remained to be the same but the variances were typically reduced by approximately 5%. Then, a direction filter [33] was applied to the simulated wave data to remove some wave interferences. Finally, the simulated shear/compressional wave speed data can be obtained. More details regarding the calculation of wave speed using simulated data can be found in our prior work [34].

3. Results

Fig. 5a (Case 1) shows that, with the increase of CPA, the estimated SWS value increased. It is worth noting that, the estimated SWS also increased with the increase of excitation frequency. This is due to the elastic shear wave scattering as reported in our previous work [35]. As shown in Fig. 5b (Case 2), the presence of steatosis reduced the group SWS values in simulated fibrotic liver tissues. Particularly, SWS values in the presence of significant (50%) steatosis did not differ significantly for tissues with 11% and 20% CPAs, as shown in Fig. 5b. Thus, differentiation of stages F3 and F4 would become more difficult.

When fibrotic livers were simulated using different CPA compositions (Case 3; see Tables 3 and 7), simulated K-Wave results are displayed in Fig. 6. Similarly, in Fig. 6a, we found that the estimated SWS values from K-Wave simulations increased with the advance of liver fibrosis from F1−F4. Also, the SWS estimates from the simulated data largely overlapped with data available in 6 peer-reviewed studies. In Fig. 6b, the probability density functions (PDFs) of the virtual SWS estimates are displayed together with PDFs generated from the computer-synthesized clinical data (subsection 3 of the Materials Section). Four PDFs of virtual SWS data were in good agreement with PDFs of "computer-synthesized" clinical SWS data. The overlaps among the 4 pairs of PFDs all exceeded 90%. In Fig. 6c, the estimated SOS values also largely overlapped the range of the SOS values clinically measured.

4. Discussion

In this study, we proposed a systems biology-inspired approach directly linking the tissue microstructures, compositions, and architectures of fibrotic livers to related ultrasound measurements such as SWS and SOS. Consequently, a significant contribution of this study was to use the proposed virtual tissue model for ultrasound-based tissue characterization. To our knowledge, this is the first biology-based discrete model designed for ultrasound tissue characterization. Although the virtual liver tissue model is simplistic, the preliminary results are encouraging. Our results suggested that the results from the K-Wave simulations were able to reproduce SWS and SOS measurements reported in the literature (Fig. 6a–c). Furthermore, results shown in Fig. 5b were consistent with a clinical study where SWE may fail to detect fibrosis in significant steatosis background [36].

Another contribution stems from the fact that the proposed research has expanded the paradigm of virtual imaging simulation [37,38]. Currently, virtual imaging simulations utilize computer-aided engineering software (*i.e.* geometry modeling and numerical modeling of image physics) to evaluate novel imaging methods without making a physical/hardware prototype. By the inclusion of the systems biology, it is possible that we can continuously simulate imaging of pathological changes due to clinical interventions. In the future, applications could include the investigation of the feasibility of monitoring of drug treatment of liver fibrosis or chemotherapy of breast cancers.

The current setting of SW simulations is close to Transient Elastography (TE) or Magnetic Resonance Elastography [1]. Acoustic radiation force-induced SWE [1] has more complex SW wavefronts and will induce (tissue) excitations with broader frequency components. Our group is in the process of extending the proposed discrete liver tissue model into an open-source elastography simulation platform [38,39] to enable more realistic ultrasound elastography simulations. In parallel, rigorous validations of the proposed discrete liver tissue model using a pre-clinical animal model will enable us to tune rules related to the systems biology simulations and conversions into mechanical properties.

There are a few limitations that should be mentioned for the sake of completeness. First, in our current K-Wave simulations [40], the wave speed (both the shear and compressional waves) and mass density values were inputs to the (shear and compressional) wave equations. Thus, both shear and compressional wave scattering is directly captured. In other words, echogenicity differences and wave energy losses due to wave scattering have been implicitly considered. However, the absorption is yet to be included and the inclusion of absorption coefficients under the framework of the K-Wave package is still in progress.

Second, only three components (*i.e.* normal liver tissue, collagen deposition, and fat) were included. However, some small structures such as small vessels were neglected and this should be considered as a limitation of this study. To our knowledge, this aspect has not been investigated in the literature. Conceptually, the presence of small

Table 7
A summary of simulation conditions.

Case No.	Simulation Conditions
1	Fibrosis without steatosis at three different CPAs 11%, 20%, and 30%) at different excitation frequencies (100–400 Hz); CL and the number of data points can be seen in Table 3.
2	Fibrosis with steatosis (50%) at three different CPAs (11%, 20%, and 30%) at different excitation frequencies (100–400 Hz); CL and the number of data points can be seen in Table 3.
3	Fibrosis without steatosis at four different METAVIR stages. The excitation frequency is at the 100 Hz. Other relevant parameters are defined in Table 3.

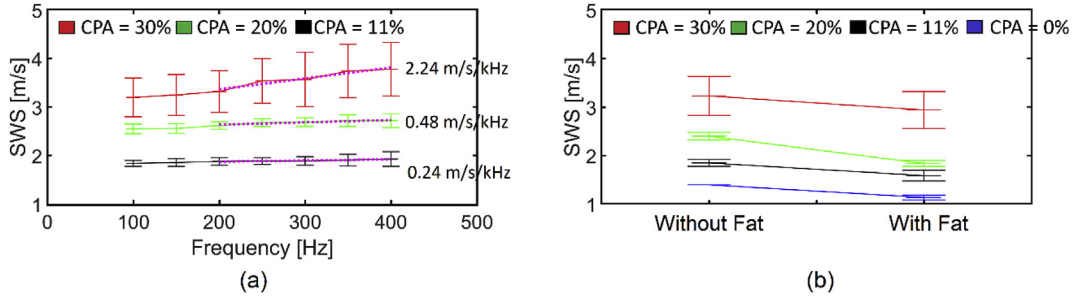

Fig. 5. In (a), plots showing mean SWS (m/s) as a function of the excitation frequency. The excitation frequencies (x-axis; 200–400 Hz) and the group SWS values (y-axis) were fitted into lines. Slopes of these lines are displayed in (a) for each stage. SWS = shear wave speed; CPA = collagen proportionate area. In (b), roughly 50% fatty lipid accumulation was simulated for F2 (11%) F3 (CPA of 20%) and F4 (CPA of 30%) stages. In (a) and (b), the error bar represents one standard deviation.

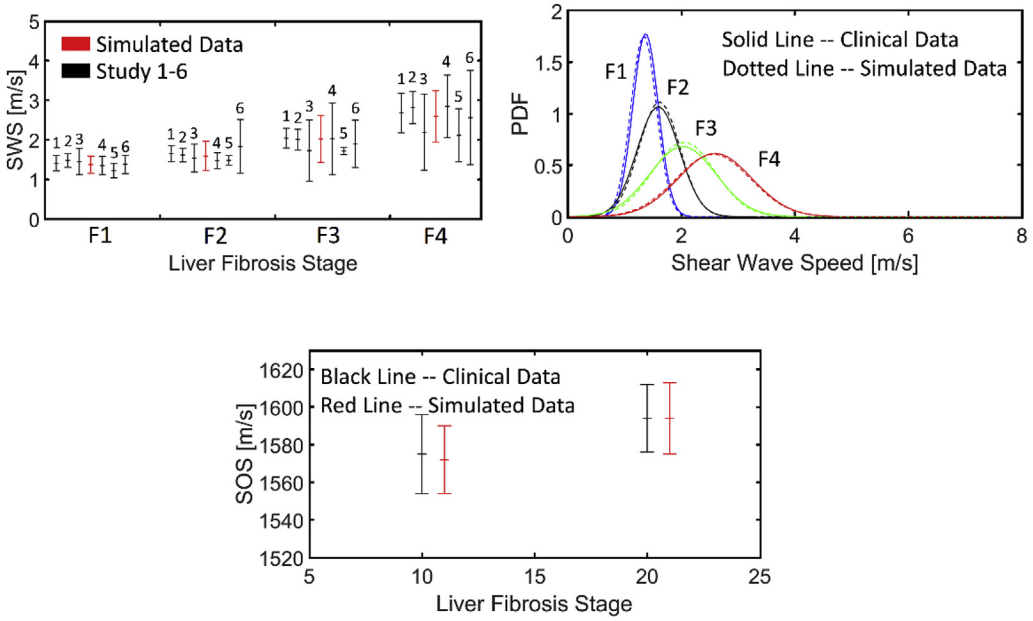

Fig. 6. Plots comparing virtual simulation data with clinically measured data for Case 9: (a) SWS values, (b) PDFs of SWS distributions, and (c) SOS values. In (a) and (c), the error bar represents one standard deviation.

vessels in the liver affects wave signals largely through additional wave scattering and therefore the measurements of SOS and SWS. In a rat model, approximately, 80% of vessels in the liver is between 10 and 20 μm [41]. Given the size of those small vessels is significantly closer to the compressional (sound) wavelength, the small vessels impact on the SOS measurements would be greater. Furthermore, in the presence of small vessels, a poroelastic material model [42] or an equivalent viscoelastic model [43] would be more appropriate. The current study used a linearly elastic model and thus, only captured the elastic wave propagation in linearly elastic heterogeneous media.

Third, clinical reports found that liver stiffness increases with hepatic inflammation [44,45], obstructive cholestasis [46] and hepatic congestion [47,48]. However, the current study did not take liver inflammation and other physiological/pathological conditions into consideration.

5. Conclusion

A systems biology-inspired discrete liver tissue model is proposed and implemented using two open-source packages (SPARK and K-Wave). We found that using the proposed discrete fibrotic liver tissue model, simulated ultrasound measurements such as SWS and SOS were comparable to those reported in the literature. Given the initial feasibility, our future work includes further refinement of the proposed tissue model. Particularly, we intend to include wave absorption and more small-scale structures such as microvasculature in the liver will be the logical next step.

Conflicts of interest

None.

Acknowledgment

This study is partially funded by a FINISHING fellowship from the Graduate School of Michigan Tech University (YW) and a research grant from the US National Institutes of Health (R15-CA179409 and R15-EB026197). The computing time was provided by Michigan Tech's Superior High-Performance Computing (HPC) cluster.

Appendix A. Supplementary data

Supplementary data to this article can be found online at https://doi.org/10.1016/j.compbiomed.2018.11.027.

References

[1] T. Shiina, K.R. Nightingale, M.L. Palmeri, T.J. Hall, J.C. Bamber, R.G. Barr, L. Castera, B.I. Choi, Y.H. Chou, D. Cosgrove, C.F. Dietrich, H. Ding, D. Amy, A. Farrokh, G. Ferraioli, C. Filice, M. Friedrich-Rust, K. Nakashima, F. Schafer,

I. Sporea, S. Suzuki, S. Wilson, M. Kudo, Wfumb guidelines and recommendations for clinical use of ultrasound elastography: Part 1: basic principles and terminology, Ultrasound Med. Biol. 41 (2015) 1126–1147.
[2] P.R. Hoskins, W. Svensson, Current state of ultrasound elastography, Ultrasound 20 (2012) 3–4.
[3] H.T. Liu, L.Z. Sun, G. Wang, M.W. Vannier, Analytic modeling of breast elastography, Med. Phys. 30 (2003) 2340–2349.
[4] R.L. Maurice, J. Ohayon, Y. Fretigny, M. Bertrand, G. Soulez, G. Cloutier, Noninvasive vascular elastography: theoretical framework, IEEE Trans. Med. Imag. 23 (2004) 164–180.
[5] S. Goenezen, J.F. Dord, Z. Sink, P.E. Barbone, J. Jiang, T.J. Hall, A.A. Oberai, Linear and nonlinear elastic modulus imaging: an application to breast cancer diagnosis, IEEE Trans. Med. Imag. 31 (2012) 1628–1637.
[6] R.J. Dewall, J. Jiang, J.J. Wilson, K.S. Lee, Visualizing tendon elasticity in an ex vivo partial tear model, Ultrasound Med. Biol. 40 (2014) 158–167.
[7] Y. Qiu, M. Sridhar, J.K. Tsou, K.K. Lindfors, M.F. Insana, Ultrasonic viscoelasticity imaging of nonpalpable breast tumors: preliminary results, Acad. Radiol. 15 (2008) 1526–1533.
[8] K.R. Nightingale, N.C. Rouze, S.J. Rosenzweig, M.H. Wang, M.F. Abdelmalek, C.D. Guy, M.L. Palmeri, Derivation and analysis of viscoelastic properties in human liver: impact of frequency on fibrosis and steatosis staging, IEEE Trans. Ultrason. Ferroelectrics Freq. Contr. 62 (2015) 165–175.
[9] J.-L. Gennisson, T. Deffieux, E. Macé, G. Montaldo, M. Fink, M. Tanter, Viscoelastic and anisotropic mechanical properties of in vivo muscle tissue assessed by supersonic shear imaging, Ultrasound Med. Biol. 36 (2010) 789–801.
[10] N.C. Rouze, M.H. Wang, M.L. Palmeri, K.R. Nightingale, Finite element modeling of impulsive excitation and shear wave propagation in an incompressible, transversely isotropic medium, J. Biomech. 46 (2013) 2761–2768.
[11] I. Sack, K. Johrens, J. Wurfel, J. Braun, Structure-sensitive elastography: on the viscoelastic powerlaw behavior of in vivo human tissue in health and disease, Soft Matter 9 (2013) 5672–5680.
[12] K.J. Parker, A microchannel flow model for soft tissue elasticity, Phys. Med. Biol. 59 (2014) 4443.
[13] K.J. Parker, J. Ormachea, S.A. McAleavey, R.W. Wood, J.J. Carroll-Nellenback, R.K. Miller, Shear wave dispersion behaviors of soft, vascularized tissues from the microchannel flow model, Phys. Med. Biol. 61 (2016) 4890.
[14] T.D. Mast, L.M. Hinkelman, L.A. Metlay, M.J. Orr, R.C. Waag, Simulation of ultrasonic pulse propagation, distortion, and attenuation in the human chest wall, J. Acoust. Soc. Am. 106 (1999) 3665–3677.
[15] K. Suzuki, N. Hayashi, Y. Sasaki, M. Kono, A. Kasahara, H. Fusamoto, Y. Imai, T. Kamada, Dependence of ultrasonic attenuation of liver on pathologic fat and fibrosis: examination with experimental fatty liver and liver fibrosis models, Ultrasound Med. Biol. 18 (1992) 657–666.
[16] T. Fujii, B.C. Fuchs, S. Yamada, G.Y. Lauwers, Y. Kulu, J.M. Goodwin, M. Lanuti, K.K. Tanabe, Mouse model of carbon tetrachloride induced liver fibrosis: histopathological changes and expression of CD133 and epidermal growth factor, BMC Gastroenterol. 10 (2010) 79.
[17] J.J. Bradley E. Treeby, Daniel Rohrbach, B.T. Cox, Modelling elastic wave propagation using the k-wave MATLAB toolbox, IEEE International Ultrasonics Symposium Proceedings, 2014.
[18] A. Solovyev, M. Mikheev, L. Zhou, J. Dutta-Moscato, C. Ziraldo, G. An, Y. Vodovotz, Q. Mi, SPARK: a framework for multi-scale Agent-based biomedical modeling, Int. J. Agent Technol. Syst. (IJATS) 2 (2010), https://doi.org/10.4018/jats.2010070102.
[19] J. Dutta-Moscato, A. Solovyev, Q. Mi, T. Nishikawa, A. Soto-Gutierrez, I.J. Fox, Y. Vodovotz, A multiscale Agent-based in silico model of liver fibrosis progression, Front Bioeng Biotechnol 2 (2014) 18.
[20] S.G. Hubscher, Histological assessment of non-alcoholic fatty liver disease, Histopathology 49 (2006) 450–465.
[21] J. Schleicher, R. Guthke, U. Dahmen, O. Dirsch, H.G. Holzhuetter, S. Schuster, A theoretical study of lipid accumulation in the liver-implications for nonalcoholic fatty liver disease, Biochim. Biophys. Acta 1841 (2014) 62–69.
[22] A.M. Diehl, Z.P. Li, H.Z. Lin, S.Q. Yang, Cytokines and the pathogenesis of non-alcoholic steatohepatitis, Gut 54 (2005) 303–306.
[23] B. Boozari, A. Potthoff, I. Mederacke, A. Hahn, A. Reising, K. Rifai, H. Wedemeyer, M. Bahr, S. Kubicka, M. Manns, M. Gebel, Evaluation of sound speed for detection of liver fibrosis: prospective comparison with transient dynamic elastography and histology, J. Ultrasound Med. 29 (2010) 1581–1588.
[24] K. Nightingale, S. McAleavey, G. Trahey, Shear-wave generation using acoustic radiation force: in vivo and ex vivo results, Ultrasound Med. Biol. 29 (2003) 1715–1723.
[25] T. Khamdaeng, J. Luo, J. Vappou, P. Terdtoon, E.E. Konofagou, Arterial stiffness identification of the human carotid artery using the stress-strain relationship in vivo, Ultrasonics 52 (2012) 402–411.
[26] B.K. Kim, S.U. Kim, G.H. Choi, W.K. Han, M.S. Park, E.H. Kim, J.Y. Park, D.Y. Kim, J.S. Choi, S.C. Yang, E.H. Choi, K. Song, S.H. Ahn, K.H. Han, C.Y. Chon, Normal" liver stiffness values differ between men and women: a prospective study for healthy living liver and kidney donors in a native Korean population, J. Gastroenterol. Hepatol. 27 (2012) 781–788.
[27] F.A. Duck, Physical Properties of Tissue: a Comprehensive Reference Book, Academic Press, San Diego, CA, USA, 1990.
[28] P. Bedossa, T. Poynard, An algorithm for the grading of activity in chronic hepatitis C. The METAVIR Cooperative Study Group, Hepatology 24 (1996) 289–293.
[29] Y. Huang, W.B. de Boer, L.A. Adams, G. MacQuillan, E. Rossi, P. Rigby, S.C. Raftopoulos, M. Bulsara, G.P. Jeffrey, Image analysis of liver collagen using sirius red is more accurate and correlates better with serum fibrosis markers than trichrome, Liver Int. 33 (2013) 1249–1256.
[30] S.H. Chen, C.Y. Peng, I.P. Chiang, H.C. Lai, C.J. Lee, W.P. Su, J.T. Kao, P.H. Chuang, Comparison of collagen proportionate areas in liver fibrosis quantification between chronic hepatitis B and C, Medicine (2016) 95.
[31] A.P. Roberts, Statistical reconstruction of three-dimensional porous media from two-dimensional images, Phys. Rev. E 56 (1997) 3203–3212.
[32] M.L. Palmeri, M.H. Wang, J.J. Dahl, K.D. Frinkley, K.R. Nightingale, Quantifying hepatic shear modulus in vivo using acoustic radiation force, Ultrasound Med. Biol. 34 (2008) 546–558.
[33] T. Deffieux, J.L. Gennisson, J. Bercoff, M. Tanter, On the effects of reflected waves in transient shear wave elastography, Ieee T Ultrason Ferr 58 (2011) 2032–2035.
[34] Y. Wang, M. Wang, J.J. Jiang, An analysis of intrinsic variations of low-frequency shear wave speed in A stochastic tissue model: the first application for staging liver fibrosis, Phys. Med. Biol. (2016).
[35] Y. Wang, M. Wang, J. Jiang, An analysis of intrinsic variations of low-frequency shear wave speed in a stochastic tissue model: the first application for staging liver fibrosis, Phys. Med. Biol. 62 (2017) 1149.
[36] A. Wieckowska, A.E. Feldstein, Diagnosis of nonalcoholic fatty liver disease: invasive versus noninvasive, Semin. Liver Dis. 28 (2008) 386–395.
[37] T. Glatard, C. Lartizien, B. Gibaud, R.F. da Silva, G. Forestier, F. Cervenansky, M. Alessandrini, H. Benoit-Cattin, O. Bernard, S. Camarasu-Pop, N. Cerezo, P. Clarysse, A. Gaignard, P. Hugonnard, H. Liebgott, S. Marache, A. Marion, J. Montagnat, J. Tabary, D. Friboulet, A virtual imaging platform for multi-modality medical image simulation, IEEE Trans. Med. Imag. 32 (2013) 110–118.
[38] Y. Wang, E. Helminen, J.F. Jiang, Building a virtual simulation platform for quasistatic breast ultrasound elastography using open source software: a preliminary investigation, Med. Phys. 42 (2015) 5453–5466.
[39] Y. Wang, B. Peng, J. Jiang, Building an open-source simulation platform of acoustic radiation force-based breast elastography, Phys. Med. Biol. 62 (2017) 1949–1969.
[40] B.E. Treeby, B.T. Cox, Modeling power law absorption and dispersion in viscoelastic solids using a split-field and the fractional Laplacian, J. Acoust. Soc. Am. 136 (2014) 1499–1510.
[41] E. Ryschich, E. Schmidt, S.M. Maksan, E. Klar, J. Schmidt, Expansion of endothelial surface by an increase of vessel diameter during tumor angiogenesis in experimental and hepatocellular and pancreatic cancer, World J. Gastroenterol. 10 (2004) 3171–3174.
[42] N. Nazari, P.E. Barbone, Shear Waves in Pressurized Poroelastic Media 141 (2017) 3720-3720.
[43] V. Morochnik, J.P. Bardet, Viscoelastic approximation of poroelastic media for wave scattering problems, Soil Dynam. Earthq. Eng. 15 (1996) 337–346.
[44] A. Sagir, A. Erhardt, M. Schmitt, D. Haussinger, Transient elastography is unreliable for detection of cirrhosis in patients with acute liver damage, Hepatology 47 (2008) 592–595.
[45] U. Arena, F. Vizzutti, G. Corti, S. Ambu, C. Stasi, S. Bresci, S. Moscarella, V. Boddi, A. Petrarca, G. Laffi, F. Marra, M. Pinzani, Acute viral hepatitis increases liver stiffness values measured by transient elastography, Hepatology 47 (2008) 380–384.
[46] G. Millonig, F.M. Reimann, S. Friedrich, H. Fonouni, A. Mehrabi, M.W. Buchler, H.K. Seitz, S. Mueller, Extrahepatic cholestasis increases liver stiffness (FibroScan) irrespective of fibrosis, Hepatology 48 (2008) 1718–1723.
[47] G. Millonig, S. Friedrich, S. Adolf, H. Fonouni, M. Golriz, A. Mehrabi, P. Stiefel, G. Pöschl, M.W. Büchler, H.K. Seitz, S. Mueller, Liver stiffness is directly influenced by central venous pressure, J. Hepatol. 52 (2010) 206–210.
[48] A. Colli, P. Pozzoni, A. Berzuini, A. Gerosa, C. Canovi, E.E. Molteni, M. Barbarini, F. Bonino, D. Prati, Decompensated chronic heart failure: increased liver stiffness measured by means of transient elastography, Radiology 257 (2010) 872–878.
[49] MonaEl-Hariri, A.G.A.E. Megid, T.F.T. Ali, MohamedHassany, Diagnostic value of Transient Elastography (Fibroscan) in the evaluation of liver fibrosis in chronic viral hepatitis C: comparison to liver biopsy, Egypt. J. Radiol. Nucl. Med. 48 (2017) 329–337.
[50] R.P. Myers, M. Elkashab, M. Ma, P. Crotty, G. Pomier-Layrargues, Transient elastography for the noninvasive assessment of liver fibrosis: a multicentre Canadian study, Can. J. Gastroenterol. 24 (2010) 661–670.
[51] J.H. Wang, C.S. Changchien, C.H. Hung, H.L. Eng, W.C. Tung, K.M. Kee, C.H. Chen, T.H. Hu, C.M. Lee, S.N. Lu, FibroScan and ultrasonography in the prediction of hepatic fibrosis in patients with chronic viral hepatitis, J. Gastroenterol. 44 (2009) 439–446.
[52] B. Coco, F. Oliveri, A.M. Maina, P. Ciccorossi, R. Sacco, P. Colombatto, F. Bonino, M.R. Brunetto, Transient elastography: a new surrogate marker of liver fibrosis influenced by major changes of transaminases, J. Viral Hepat. 14 (2007) 360–369.
[53] C.H. Liu, C.C. Liang, K.W. Huang, C.J. Liu, S.I. Chen, J.W. Lin, P.H. Hung, H.B. Tsai, M.Y. Lai, P.J. Chen, J.H. Chen, D.S. Chen, J.H. Kao, Transient elastography to assess hepatic fibrosis in hemodialysis chronic hepatitis C patients, Clin. J. Am. Soc. Nephrol.: CJASN 6 (2011) 1057–1065.
[54] J.K. Kang, J.Y. Cheong, S.W. Cho, J.H. Cho, J.S. Park, Y.B. Kim, D.J. Kim, S.G. Hwang, J.M. Yang, Y.N. Park, [Liver stiffness measurement for the diagnosis of hepatic fibrosis in patients with chronic viral hepatitis], Korean J. Hepatol. 13 (2007) 521–529.

Yu Wang received his B.S. degree in Mechano-electronics Engineering from Wuhan Institute of Technology, China, in 2010, and an M.S. in Mechano-electronics from Huazhong University of Science and Technology, China, in 2013. He graduated with a Ph.D. in Biomedical Engineering from Michigan Technological University. Currently, he is employed by Delphi Automotive Inc. His research interests include signal processing and medical ultrasound.

Jingfeng (JJ) Jiang received the BS and MS degrees in structural engineering from Zhejiang University, China, in 1995 and 1998, respectively. He obtained his MS in Computer Science and Ph.D. in Civil Engineering in 2002 and 2003 from University of Kansas, respectively. He was with the Department of Medical Physics at University of Wisconsin-Madison from 2003 to 2012, first as a post-doctoral associate and then as a research scientist. He is now an Associate Professor of Biomedical Engineering at Michigan Technological University, Houghton, Michigan. His overall research interests stride the borders among imaging, biology, and computational sciences. At the University of Wisconsin, he mainly worked on algorithm developments for ultrasound elastography. More recently, he has expanded his research into advanced open-source elastography simulations (https://github.com/jjiang-mtu/virtual-breast-project), cardiovascular flow analytics and medical imaging analysis.